

Research Article

On the Rotor Stator Interaction Effects of Low Specific Speed Francis Turbines

Einar Agnalt , Igor Iliev, Bjørn W. Solemslie , and Ole G. Dahlhaug

Waterpower Laboratory, Department of Energy and Process Engineering, NTNU-Norwegian University of Science and Technology, Trondheim, Norway

Correspondence should be addressed to Einar Agnalt; ainer.agnalt@ntnu.no

Received 16 November 2018; Revised 17 January 2019; Accepted 30 January 2019; Published 3 March 2019

Academic Editor: Ryoichi Samuel Amano

Copyright © 2019 Einar Agnalt et al. This is an open access article distributed under the Creative Commons Attribution License, which permits unrestricted use, distribution, and reproduction in any medium, provided the original work is properly cited.

The rotor stator interaction in a low specific speed Francis model turbine and a pump-turbine is analyzed utilizing pressure sensors in the vaneless space and in the guide vane cascade. The measurements are analyzed relative to the runner angular position by utilizing an absolute encoder mounted on the shaft end. From the literature, the pressure in the analyzed area is known to be a combination of two effects: the rotating runner pressure and the throttling of the guide vane channels. The measured pressure is fitted to a mathematical pressure model to separate the two effects for two different runners. One turbine with 15+15 splitter blades and full-length blades and one pump-turbine with six blades are investigated. The blade loading on the two runners is different, giving different input for the pressure model. The main findings show that the pressure fluctuations in the guide vane cascade are mainly controlled by throttling for the low blade loading case and the rotating runner pressure for the higher blade loading case.

1. Introduction

The rotor stator interaction (RSI) is known to be the main source for pressure fluctuations in low specific speed turbines. The pressure from the rotating runner causes pressure fluctuations in the vaneless space, guide vane cascade and farther upstream in the spiral casing and the inlet conduit. This phenomenon has been thoroughly investigated for decades in hydraulic machinery. In the open literature, various terms are used to describe the effects of the RSI, such as throttling, blocking, potential interaction, rotating runner pressure field, and squeezing. The throttling and blocking are the effects creating the fluctuating pressure and velocity in the guide vane cascade. The source of the fluctuations is the downstream runner with high- and low-pressure sides of the blades giving fluctuations in the downstream boundary condition of each guide vane passage. The potential interaction is the combination of the two pressure fields in the rotor and stator. The rotating pressure field is the high and low pressure onboard the runner due to the blade loading, seen from the stationary domain, and the stationary pressure field is the high and low pressure around each guide vane.

Several studies focus on how the RSI fluctuations in Francis runners and pump runners affect the surroundings of the runner and how to predict the pressure fluctuations, but details about the RSI effects are not discussed [1–3]. Zobeiri et al. [4] focused on the pressure propagation of the RSI in the guide vane cascade and the spiral casing in a pump-turbine in generating mode. The presented results showed how the rotor stator interaction created pressure fluctuations in the monitored area. By investigating the presented figures, the highest pressure was found when the high-pressure side of the impeller was near the measuring sensor. In the guide vane cascade, the highest pressure was found when the high-pressure side of the impeller was in the same location as the guide vane trailing edge stagnation pressure. In addition, an observation of a higher harmonic can be seen in the measurements without further discussion. Yonezawa et al. [5] showed how the RSI interacted with the penstock waves and created a resonance condition. The unsteady pressure propagating upstream the runner was strongly connected to the rotor stator interaction through the throttling effect. Qian [6], Ciocan and Kueny [7], and Hasmatuchi [8] did detailed studies of the velocity field in the vaneless gap and

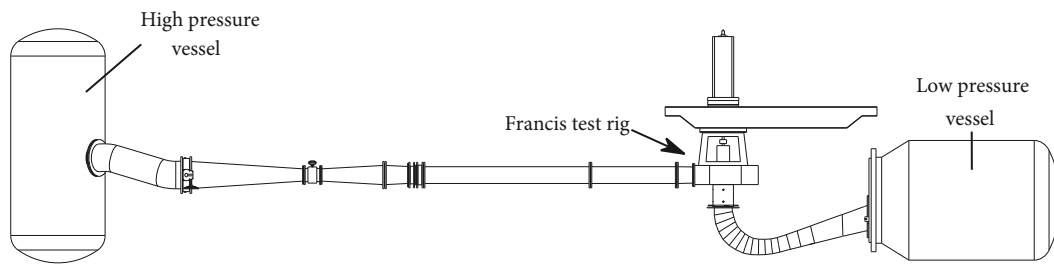


FIGURE 1: The Francis test-rig, including the high and low pressure vessels. The figure is reproduced from Agnalt et al. 2018 [12].

the guide vane cascade. Major findings were how the runner blades created a blockage of the flow in the guide vanes thereby creating a velocity fluctuation in the entire guide vane cascade, and details about the velocity field in the guide vane cascade could be seen. Other explanations found in the literature for the RSI include a “shock” created when the blade leading edge is in the vicinity of a guide vane trailing edge and the different amplitudes found in the vaneless space is explained with squeezing of water towards the guide vanes.

Based on the findings in the literature, the RSI in the vaneless gap and in the guide vane passages can be seen as a combination of two effects, namely, the throttling of the flow in the guide vane passages and the rotating pressure field from the runner. Both effects originate from the rotating pressure field, but the throttling of the guide vane passages creates pulsations in the velocity field, in and upstream the guide vane cascade, which could create a hydroacoustic resonance condition. The rotating pressure field would decay exponentially with the distance from the runner if there were no guide vanes, and the throttling of the guide vane channels is the effect creating upstream fluctuations [9].

The current paper presents pressure measurements in the vaneless space to investigate the physics of the RSI. To enable a detailed analysis, three sensors were utilized in the vaneless space and one in the guide vane cascade to distinguish between the throttling and the rotating pressure field effects. The throttling effects were assumed to be in phase for the pressure sensors in the same guide vane channel, while the pressure field rotating with the runner was phase shifted corresponding to the position of the pressure sensors. From these assumptions, a mathematical pressure model was developed to analyze both effects. The purpose of the pressure model is to detect both the various amplitudes and the phase shifts measured in the pressure field in the vaneless space. The main objective of the current study is to decompose the measured pressure in the effect of throttling and the rotating pressure field to increase the details and the precision in the understanding of the rotor stator interaction effects.

2. Methods

2.1. Experimental Setup. The Francis test-rig available at the Waterpower Laboratory, Norwegian University of Science and Technology, was used for the experimental studies [10]. The Francis test-rig was equipped with all required instruments to conduct model testing according to IEC 60193

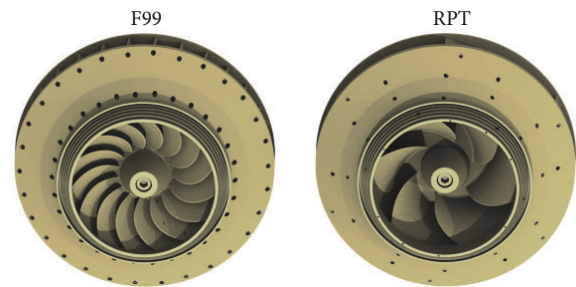


FIGURE 2: Three-dimensional view of the investigated runners.

[11]. The number of guide vanes was 28 and the spiral casing was bolted through 14 stay vanes. The draft tube of the test-rig was an elbow-type. The Francis turbine in the test-rig is shown in Figure 1 [12].

Measurements were performed on two runners in the Francis test-rig. First a bolted design with 15+15 splitter and full-length blades was utilized in the Francis 99 research project [10], denoted F99, and second a reversible pump-turbine, denoted RPT, with six blades as shown in Figure 2. The F99 runner has dimensionless specific speed of 0.07 and the RPT 0.08. Both runners were designed to fit the same test-rig; hence, main dimensions were equal. The F99 runner was based on the Tokke power plant in Norway and was developed to provide measurements on an open geometry to the hydropower research community. The RPT was designed to study the instable behavior at part-load for low specific speed pump-turbines [13].

Flush mounted sensors were selected to reduce uncertainty related to the mounting method [14]. Figure 4 shows the locations of the pressure sensor in the turbine (S1 to S4). All sensors were bridge sensors directly connected to the data acquisition (DAQ) system with excitation voltage from the DAQ module. The position sensor was installed on the end of the shaft, above the generator as shown in Figure 3. The signal was converted to analog $\pm 10V$ before the DAQ system with a digital to analog converter (DAC) to utilize synchronized parallel sampling with the signals from the pressure sensors.

2.2. Measurements. The results in this paper are based on the measurements conducted at the operational points presented in Table 1. Several guide vane openings were investigated, but the results were similar and the best efficiency points (BEP)



FIGURE 3: Absolute position sensor on the shaft end above the generator.

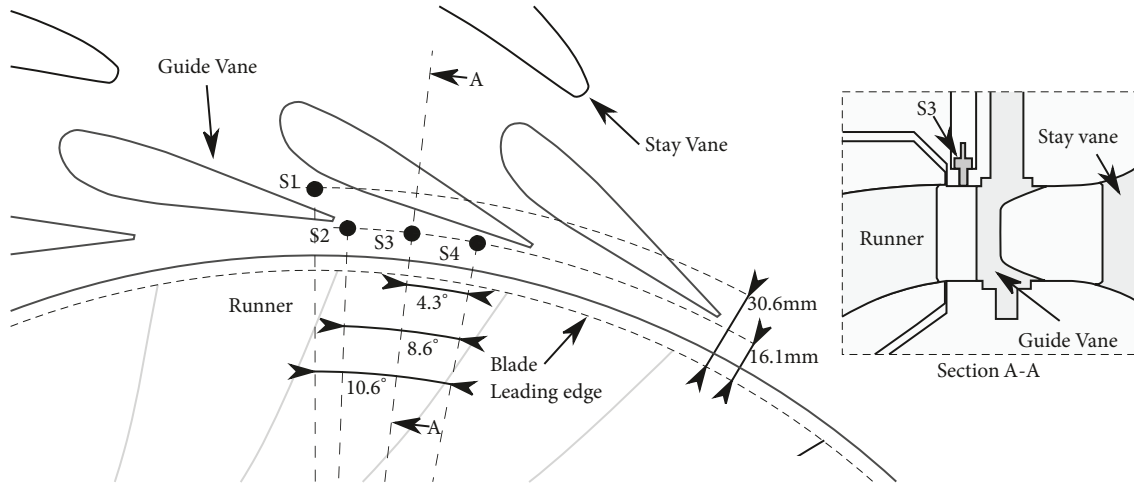


FIGURE 4: Pressure sensors in the vaneless space and in the guide vane cascade. The angular distance between sensor S2-S3 and S3-S4 is 4.3° . The sensors were flush mounted in the upper cover of the turbine as shown with sensor S3 in section A-A. The distances from the runner blades leading edges to the sensors are 16.1mm and 30.6mm.

for both runners were selected to have the best signal to noise ratio.

2.3. Calibration and Uncertainty. Static calibration of the pressure sensors was initially done in an estimated pressure range for the measurements with a GE P3000 Series pneumatic deadweight tester as the primary reference. As evaluation of pressure amplitudes is a dynamic quantity, dynamic uncertainty must be addressed. All components in the current pressure measurement chain, from the sensors to the data acquisition, are stated to have resonance frequencies above 10kHz; hence, the dynamic uncertainty is assumed to be neglectable and only repeatability and hysteresis from static calibration remain in the uncertainty evaluation. A repeatability test was conducted at 1 Hz with a pressure alternating between 100kPa and 90kPa absolute pressure. The uncertainty budget for the RSI blade passing amplitudes at BEP is shown in Table 2.

The uncertainty budget for the position sensor (Z) is summarized in Table 3. The uncertainties are based on the given data for the encoder and the DAC. A smoothing filter was utilized to filter the signal noise, and the noise uncertainty was calculated from the difference in the raw signal and the filtered position signal used in the analysis [15]. Timing uncertainties were converted to angular offset with the average of the speeds given in Table 1.

The position accuracy was verified with several measurements at BEP, at different rotational speed and head. The angular shift of the pressure was calculated with cross-correlation and was found to be within the stated total absolute uncertainty.

2.4. Pressure Model. All pressure values presented were calculated as percentage of specific hydraulic energy of the machine ($E=gH$) and denoted $pE(\%)$ as recommended by the IEC60193 [11] where H is net head. The pressure fluctuations in the vaneless space and guide vane channels were assumed to be a linear combination of a rotating runner pressure field (\tilde{p}_r) and a variation in the guide vane cascade pressure due to throttling of the respective guide vane channel (\tilde{p}_b). The total pressure fluctuation measured in each location (\tilde{p}_t) was the superposition of the runner pressure and the guide vane channel pressure; hence, a two-way coupling was not considered. All measured pressures were modelled as a sum of sines and as a function of the runner position, x . The frequencies (f) were normalized to the runner rotational frequency and harmonics were denoted i for each sensor (k). A phase offset $\delta_{k,i}$ was introduced to set the start position of each harmonic. The amplitudes ($a_{k,i}$) were independent for each sensor and each harmonic.

$$\tilde{p}_{t,k} = \tilde{p}_{r,k} + \tilde{p}_{b,k} = \sum_i a_{k,i} \cdot \sin(i \cdot f \cdot x + \delta_{k,i}) \quad (1)$$

TABLE 1: Measurement summary. α is guide vane opening as defined in the IEC60193 [11].

Description	n_{ED}	Q_{ED}	Head	α	Flow	Efficiency	Speed
F99, BEP	0.180	0.154	15.6m	10°	0.232m ³ /s	92.2%	382.2 rpm
RPT, BEP	0.220	0.134	12.0m	11°	0.185m ³ /s	89.1%	412.7 rpm

TABLE 2: Uncertainty budget for RSI first and second harmonic amplitudes, BEP F99.

Sensor	1Hz Repeatability [kPa]	Amplitude RMS of first harmonic RSI [kPa]	Relative Uncertainty [%]	Amplitude RMS of second harmonic RSI [kPa]	Relative Uncertainty [%]
S1	0.002	0.404	0.50	0.028	7.2
S2	0.005	0.462	1.1	0.018	28
S3	0.002	1.218	0.16	0.064	3.1
S4	0.002	1.118	0.18	0.098	2.0

TABLE 3: Uncertainty budget of position sensor.

Encoder linearity [°]	DAC conversion rate [°]	Noise [°]	Time delay [°]	Total absolute uncertainty [°]
0,05	0	0,4	0,2	0,45

For the throttling pressure, the measurements in each sensor position were in the same guide vane channel; hence, each harmonic of the pressure for all sensors was assumed to have the same phase. A harmonic phase offset (γ_i) was utilized for the start position of the pressure. The amplitudes ($b_{k,i}$) were independent for each sensor and each harmonic.

$$\tilde{p}_{b,k} = \sum_i b_{k,i} \cdot \sin(i \cdot f \cdot x + \gamma_i) \quad (2)$$

The runner pressure was assumed equal for each measurement position. Due to the rotation of the runner, the phases were set equal to the sensor angular offset (θ_k). An additional parameter (φ_i) was introduced to allow phase position adjustment of each harmonic. The amplitudes (c_i) were independent for each harmonic, but in common for each sensor.

$$\tilde{p}_{r,k} = \sum_i c_i \cdot \sin(i \cdot f \cdot x + \varphi_i - i \cdot f \cdot \theta_k) \quad (3)$$

The equation for the total pressure fluctuation was (2) and (3) inserted into (1)

$$\begin{aligned} \tilde{p}_{t,k} &= \sum_i b_{k,i} \cdot \sin(i \cdot f \cdot x + \gamma_i) + \sum_i c_i \cdot \sin(i \cdot f \cdot x + \varphi_i - i \cdot f \cdot \theta_k) \\ &= \sum_i a_{k,i} \cdot \sin(i \cdot f \cdot x + \delta_{k,i}) \end{aligned} \quad (4)$$

The total number of unknowns was $i \cdot (2 \cdot k + 1)$ and the number of constants was $i \cdot (k + 3)$ as a function of the number of harmonics and the number of sensors calculated. However, (4) with more than one harmonic gave more than one solution; hence, a stepwise calculation was performed. The first harmonic was solved initially, then the next harmonic with the previous as constants as shown in Table 4.

3. Results and Discussion

The following steps were performed:

- (1) Presentation of the measurement data
- (2) Analysis of the amplitude and phase information in the measured data with least square fitting to a sum of sines, (1)
- (3) Analysis of the effect from throttling and rotating pressure with least square fitting, (4)
- (4) Comparison of the calculated throttling effect with the measurement S1

The measurements were analyzed relative to the position of the runner, which was discretised into 720 angular sectors and the data from 600 revolutions was analyzed in each sector. The details about the analysis method were published in a previous paper [15]. In order to compare the phase shifts with the position relative measurements, it was converted to runner angular position change. The relation between the runner angular position (θ) and the pressure phase shift (ϕ) of the harmonic (i) of a normalized frequency (f) is

$$\phi = \theta \cdot i \cdot f \quad (5)$$

The pressure in the vaneless space was measured with sensors S2 to S4 and the pressure in one guide vane channel with the sensor S1. The sensor S1 was utilized as a reference for the throttling phase with the assumption of pure throttling effect inside a guide vane channel. The sensors S2-S4 were used for the calculations of the pressure model. The measurements were high pass filtered at half the blade passing frequency to remove the lower frequency effects.

In Figure 5, the pressure measured with the sensors S1 and S2 fluctuated in phase for both the F99 and the RPT. This

TABLE 4: Stepwise calculation of pressure field.

Fit	Formula	Fit coefficients	Constants
j=1	$c_{k,1} \cdot \sin(1 \cdot f \cdot x + \varphi_1 - 1 \cdot f \cdot \theta_k) + b_{k,1} \cdot \sin(1 \cdot f \cdot x + \gamma_1) = a_{k,1} \cdot \sin(1 \cdot f \cdot x + \delta_{k,1})$	$c_1, \varphi_1, b_{k,1}, \gamma_1$	$a_{k,1}, \delta_{k,1}, \theta_k$
j>1	$\sum_{i=1}^{j-1} [c_i \cdot \sin(i \cdot f \cdot x + \varphi_i - i \cdot f \cdot \theta_k)] + c_j \cdot \sin(j \cdot f \cdot x + \varphi_j - j \cdot f \cdot \theta_k) + \sum_{i=1}^{j-1} [b_{k,i} \cdot \sin(i \cdot f \cdot x + \gamma_i)] + b_{k,j} \cdot \sin(j \cdot f \cdot x + \gamma_j) = \sum_{i=1}^j [a_{k,i} \cdot \sin(i \cdot f \cdot x + \delta_{k,i})]$	$c_j, \varphi_j, b_{k,j}, \gamma_j$	$a_{k,1}, \delta_{k,1}, \dots$ $a_{k,j}, \delta_{k,j}$ θ_k $c_1, \varphi_1, b_{k,1}, \gamma_1, \dots$ $c_{j-1}, \varphi_{j-1}, b_{k,j-1}, \gamma_{j-1}$

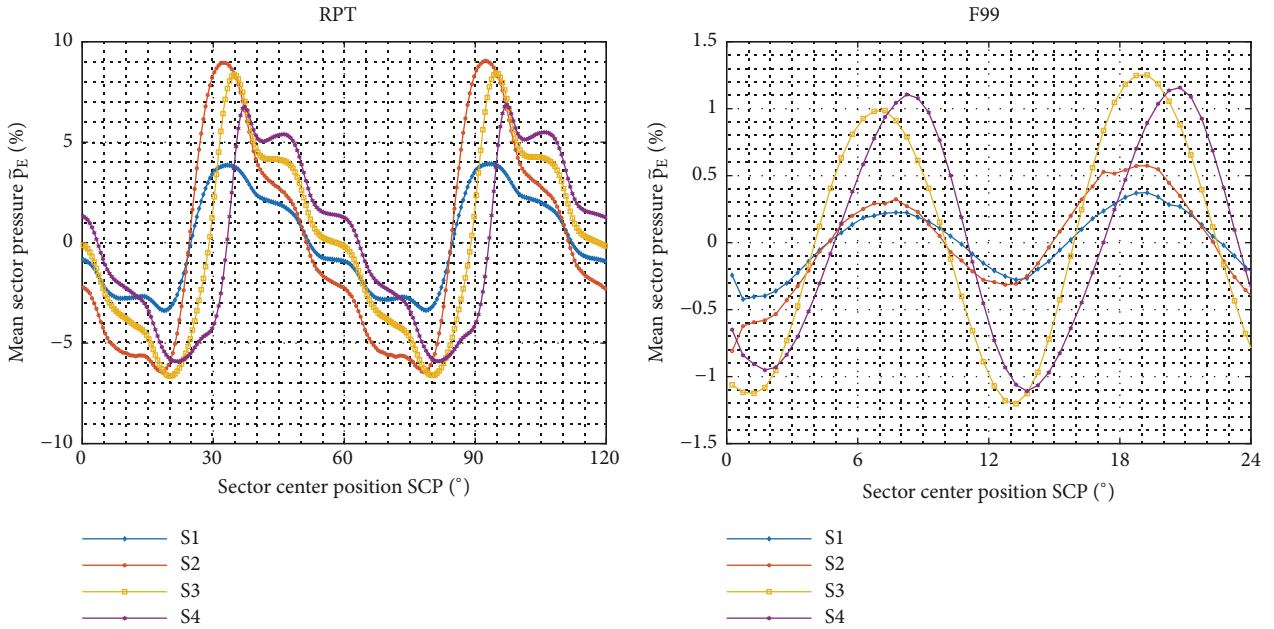


FIGURE 5: The mean sector pressure from the pressure sensors as percentage of specific energy. The angular size of each sector was 0.5° , with 720 sectors in total. The mean sector pressure was calculated from 600 full revolutions.

was similar to the results found in the literature described as throttling. For the sensors S2 to S4, the measurements were not according to pure throttling nor pure rotational pressure. In the F99 case, the pressure at S4 was lagging compared to S1 to S3, while the RPT measurements had lagging close to the angular shift of the pressure sensors (θ). In addition, the amplitudes in the different sensor locations were varying for the F99, while the RPT amplitudes were in the same range, especially for S2-S4 in the vaneless space. From the measurements, the F99 seemed mostly affected by the throttling, while the RPT was mainly affected by the rotating runner pressure field.

The amplitudes and phases of the measured signals were found by fitting the measured data to (1). The fitting algorithm was a gradient based minimizer. The F99 measurements were fitted with half the blade passing frequency (the splitter effect), the first and the second harmonics. The RPT was fitted

with the first harmonic blade passing frequency and up to and including the fifth harmonic. The highest fit accuracy for the RPT was achieved with eight harmonics, but only the first five were included to limit the results. The fitting results of the measured pressure for S2 and S3 are presented in Figure 6. It can be seen that the higher harmonics of the RTP have a small deviation between the fit and the measured signal, but the results were still found satisfactory. The F99 had good agreement between the fits and the measurements. Some deviation was expected since the fit acts as a filter, only keeping the RSI frequencies. The accuracy of the results for S1 was similar to S2, and the accuracy of the S4 results was similar to S3.

The calculated phases from the measurement fitting are presented in Figure 7. The sensors location shifts are indicated with the stems and the measured phase shifts for each harmonic with the bars.

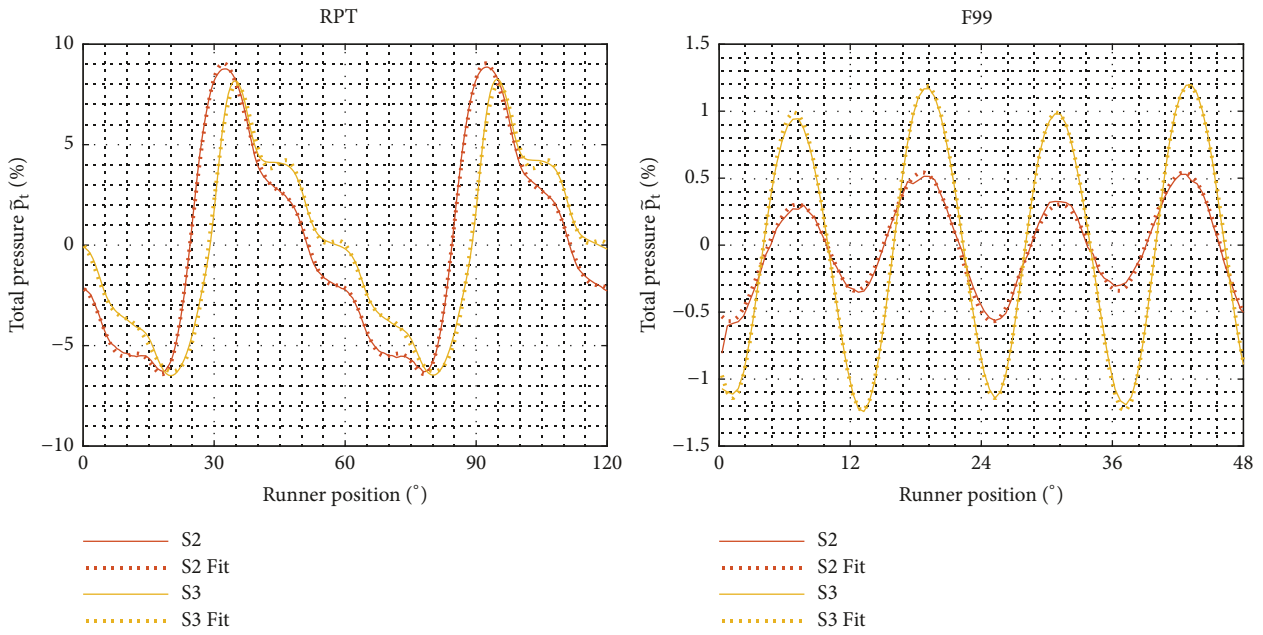


FIGURE 6: The measured signal and the fit represented with the measurements from sensor S2 and S3.

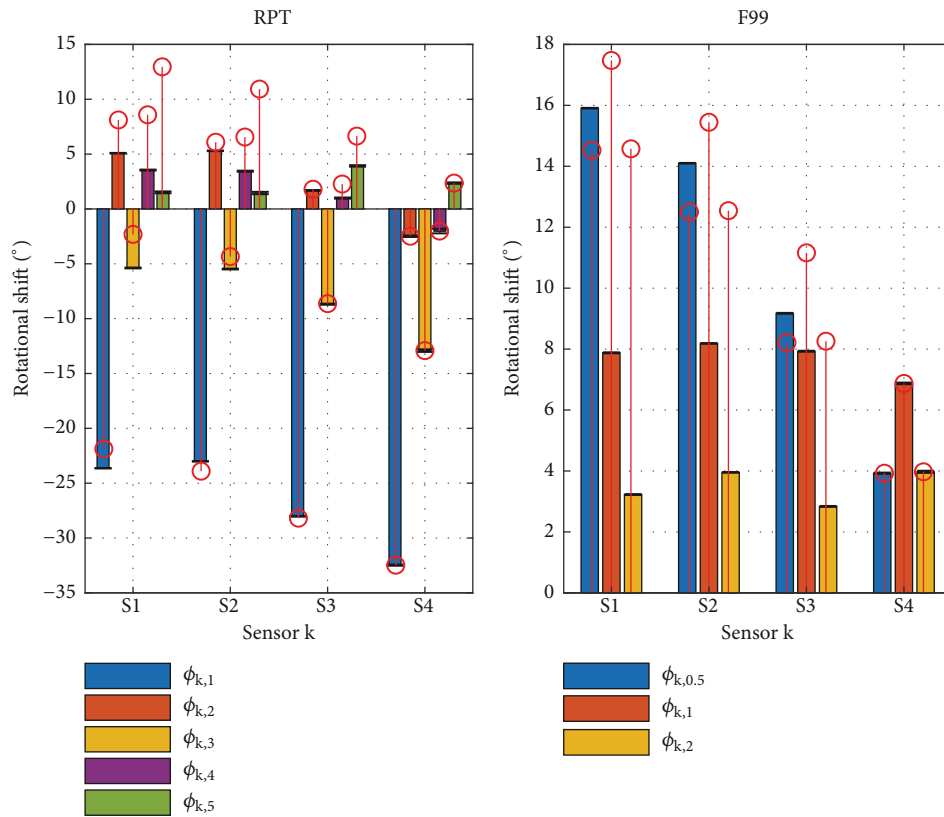


FIGURE 7: The angular shift from S4 to S1, S2, and S3 relative to runner rotation. The theoretical shift according to the sensor position as shown in Figure 4 is indicated with the red stems. The theoretical shift is normalized to sensor position S4. The subscript k is the sensor number S1 to S4.

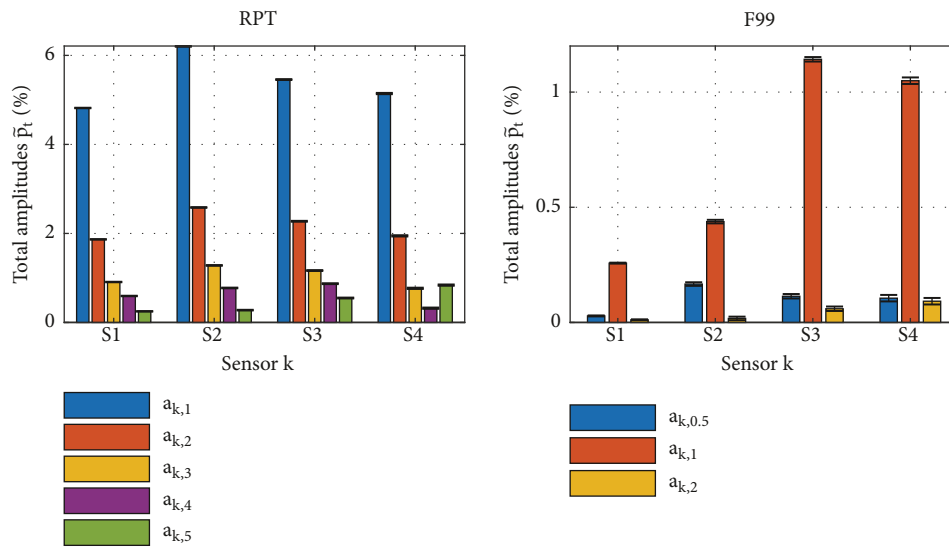


FIGURE 8: The blade passing frequency amplitude with 95% probability for each sensor. The amplitude is percentage of specific energy. The subscript k is the sensor number S1 to S4.

A pure throttling effect would result in all measurements being in phase and a pure rotating pressure effect would give phases similar to the position of the pressure sensors. The phase results presented coincide with the observation in Figure 5.

The difference between the sensor angular position and the measured phase is now discussed. For the pressure measured with sensor S1, the difference was a consequence of the position inside a guide vane channel, and thereby mainly throttling was measured. For the RPT case, the fundamental and two next harmonics ($k=1,2,3$) were close to the theoretical shift, the fourth ($k=4$) had about half the theoretical shift and the fifth ($k=5$) was found with almost the same phase for all sensors. This gave reasons to believe that the first three ($k=1,2,3$) harmonics were controlled by throttling, the last ($k=5$) by the rotating pressure field and the fourth ($k=4$) by both throttling and the rotating pressure field.

For the F99 case, the two blade passing frequency harmonics ($k=1-2$) were not following the sensor angular shift. Compared with the results from the RPT, the F99 seemed to be controlled by the throttling effect since the phase shift between the sensors was relatively small. The half blade passing frequency ($k=0.5$) had a phase difference close to the theoretical shift. The effect is known to be due to the splitter design causing slightly different flow conditions in two neighboring channels. As a result, the pressure changed for each second blade passing and the effect was therefore strongly connected to the runner position and the rotational shift.

The fitting results of the measured amplitudes are shown in Figure 8. The amplitudes from the throttling effect were unknown, as the velocity around the guide vanes was location dependent and thereby the pressure amplitudes location was dependent too. For the rotating pressure, the assumption was to find the same amplitude for all sensors at the same distance from the runner (S2-S4). The data in Figure 8 confirms the

observations from the phase. The RPT had similar amplitudes for each sensor compared with the F99 with more variations, indicating most throttling for the F99 case.

The next step was to separate the two effects. The amplitudes and phases were used to solve (4). The square error of the equation was minimized in five steps for the RPT and in three steps for the F99 according to Table 4. The calculation results for each step are shown in Figure 9. The results are presented with the throttling, the rotating runner pressure and the comparison between the total modelled pressure and the measured pressure for S2-S3. For the RPT, Fit I is the blade passing frequency ($i=1, f=6$) and the last calculation was Fit V for the fifth harmonic. The rotating runner pressure was found to be the predominant effect with the highest amplitudes, as expected from the phase discussion. The throttling was highest when the blade passed the guide vane channel, and almost no effect was found before the next blade passing. This was expected since the throttling was driven by the sudden increase in the downstream pressure from the high-pressure side of a blade. Another observation is the harmonic content of the pressure. The throttling did only have the three first harmonics, while the rotating pressure field was found with all harmonics. This was in accordance with the observation of the phase where the higher harmonics seemed to be more influenced by the rotating pressure. Initially, all harmonics for the rotating pressure were fitted with phase shift according to the sensor location as previously described. However, with such assumption the Fit V did not change from Fit IV. Due to the low number of blades, the pressure fluctuations onboard the runner were expected to be found in the vaneless space measurements as seen in the literature [4]. In the current experiment with six blades and 28 guide vanes, four guide vane passages should occur with S1-S4 still in the same runner channel. The pressure effects onboard the runner from these passages should be in phase for all pressure sensors. The number of blades and guide

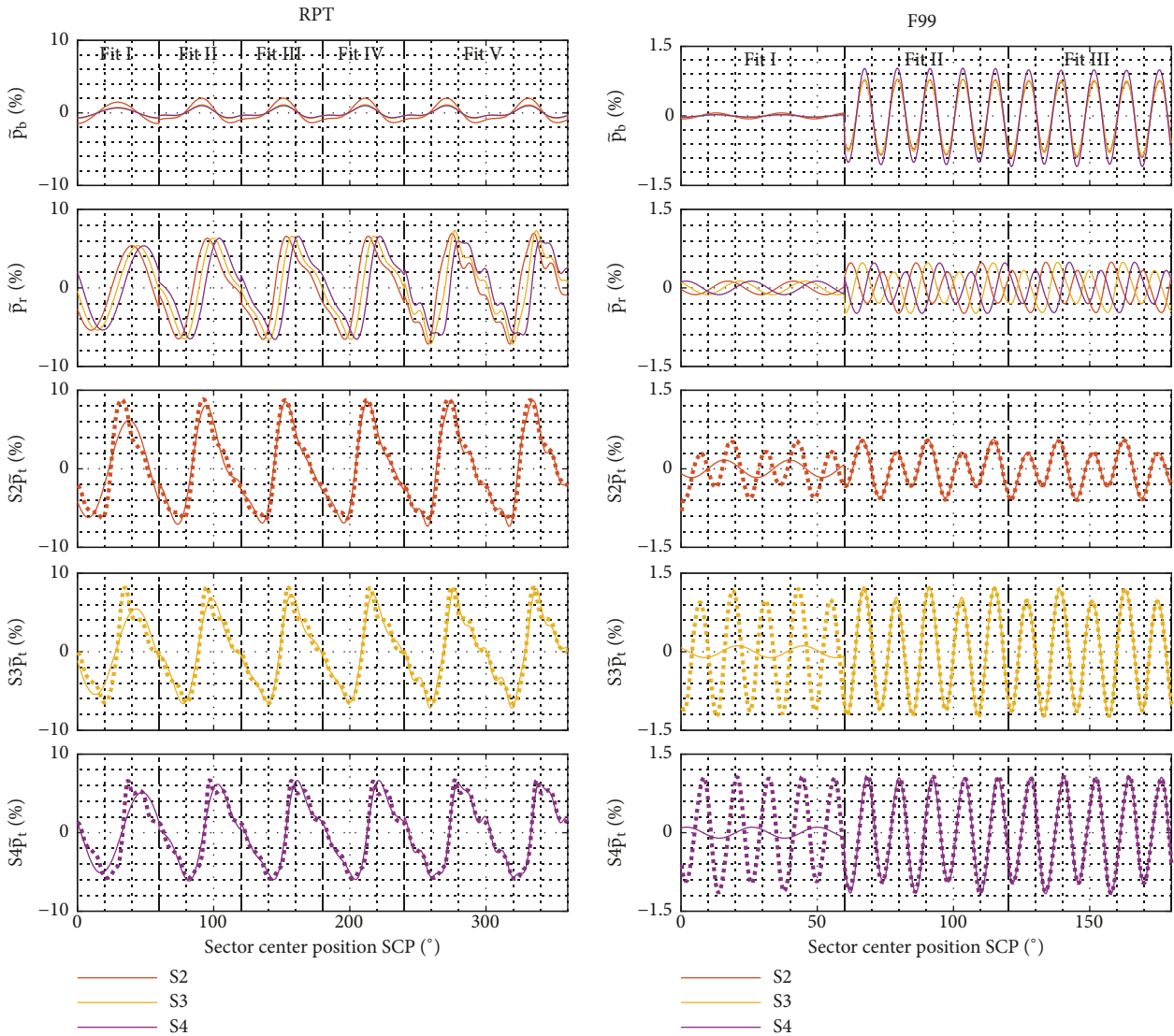


FIGURE 9: The fitting results. The results are divided into the throttling effect, the runner pressure effect, and the total pressure in each location S2-S4.

vanes made this pressure coincide with the fifth harmonic. In the initial fitting process, the fifth harmonic did not improve the fit when modelled with a phase shift according to (3). In the Fit V in Figure 9, the fifth harmonic was assumed in phase for all sensors, significantly improving the fit. From this result, the onboard pressure fluctuations could be analyzed with sensors in the vaneless space. This should be analyzed in a future study, with both onboard sensors and sensors in the vanless space of a runner with sufficiently few blades.

The F99 was initially fitted with half the blade passing frequency ($i=0.5$, $f=30$) and then the first and the second harmonic. It can be observed that the fit improved for each step. The throttling in the F99 case was the most predominant part of the measurement, which also explained why the measurements S1-S4 were almost in phase. The splitter effect did have a small influence of the throttling, obviously because

of the slightly different amplitude of the high pressure from the runner.

The position of the runner with the highest throttling and highest pressure for S2-S3 is shown in Figure 10 for the RPT case. The maximum pressure order was found to be first throttling, then S2, S3 and S4, i.e., in the order of the sensor position. This was as expected with the highest influence from the rotating runner pressure. The rotational shift of the blades for each peak can be observed. The runner does not rotate the same distance as the sensors position between each maximum. This difference is due to the throttling effect.

For the F99 case, the position of the runner for the highest pressure in throttling and each pressure measurements is shown in Figure 11. Interestingly, the order was first S2, then S3, throttling and last S4. The throttling effect is evident from the small rotational shift of the runner between the maximum pressures as seen from the position of the blades.

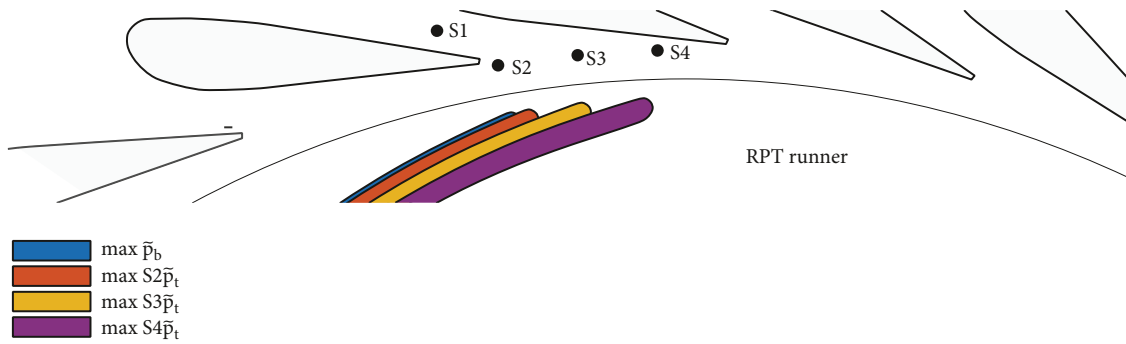


FIGURE 10: The blade positions for the RPT where the highest effect was found from throttling and the measured total pressure in the location S2-S4.

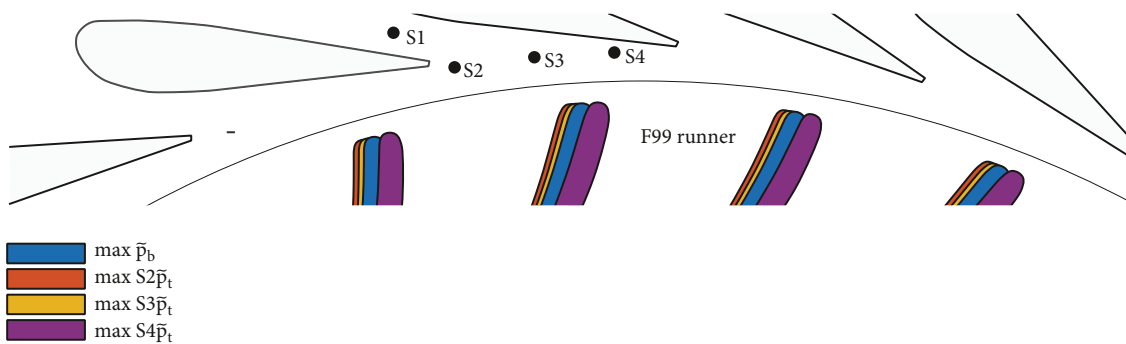


FIGURE 11: The blade positions for the F99 where the highest pressures were found.

To verify the calculated phase for the throttling, it was compared with the measurement S1 as shown in Figure 12. Both RPT and F99 had good agreement between the calculated throttling and the measurement at the location S1. The amplitude was a function of location dependent; thus, they were not expected to be comparable and therefore normalized to max.

The RPT measurements, with high blade loading and few blades, gave the most expected result. First, throttling of a guide vane channel was seen when the high-pressure side of the blade was in the vicinity of the stagnation pressure of the trailing edge of the first guide vane as shown in Figure 10. Next, the high pressure from the runner was measured in the same order as the position of the sensors in the vaneless space. The throttling effect caused the phase shift of the measurements to be smaller than the actual distance between the sensors. In the case of F99, the blade loading was smaller, giving amplitudes in the vaneless space of 1/5 of the RPT as seen in Figure 9. This is believed to be the main cause of the different order in Figure 11 compared to the RPT in Figure 10. The pressure in the guide vane cascade was much stronger compared to the rotating runner pressure; hence, the main effect in the measurements was from the throttling, which was the fluctuation of the cascade pressure. The reason for the position of the highest effect of throttling was believed to be where the pressure difference between the runner and the guide vane is the highest, hence between two trailing edges as seen in Figure 11. From airfoil theory, a known strong

connection between the pressure distribution around the airfoil and the velocity field exists [16]. The throttling effect is understood to be a consequence of increasing the pressure on the low-pressure side of the airfoil. By disturbing the pressure field, both velocity and pressure around that particular guide vane were disturbed.

4. Conclusion

Two runners with similar specific speed but different number of blades were investigated to find the effects from the rotor stator interaction in the vaneless space. For the F99 case with lowest blade loading, the main influence of the pressure field in the guide vane cascade and vaneless space was found to be the pressure disturbance from the runner introducing a throttling effect in the guide vane channel, resulting in fluctuation in the potential pressure in the guide vane cascade. The findings are in accordance with previous studies found in the literature [6–8].

With higher blade loading and few blades, the pressure in the vaneless space was a direct measurement of the rotating pressure field from the runner and small influence from the throttling as with the RPT case.

The fifth harmonic in the RPT case was found to be the onboard pressure fluctuations because the wide channel gave the possibility of measuring several guide vanes passing with the sensors in the vaneless space.

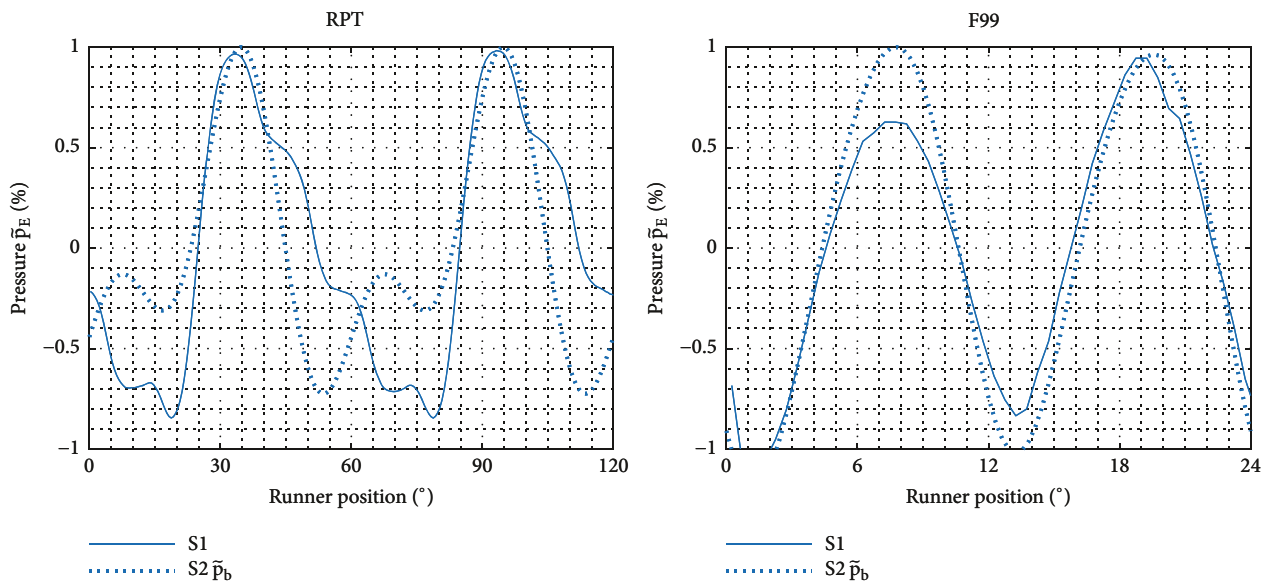


FIGURE 12: Comparison of the calculated throttling pressure and the measurements with sensor S1. All pressure values were normalized to signal max.

The throttling effect was found in different locations for the two cases and is highly influenced by the blade loading. The higher blade loading gave highest throttling when the high-pressure side of the blade was close to the guide vane channel outlet, while lower blade loading moved the throttling position closer to the low-pressure area of the guide vanes.

The difference in the measured pressure amplitudes in the vaneless space was caused by the phase shift between the throttling effect and the rotating runner pressure and their amplitudes.

The results give more details about the physics in the rotor stator interaction in a low specific speed turbine.

Nomenclature

a	: Amplitude total pressure
b	: Amplitude throttling pressure
c	: Amplitude runner pressure
f	: Normalized frequency
i	: Harmonic number
n_{ED}	: Dimensionless speed factor
\bar{p}	: Fluctuating pressure
Q_{ED}	: Dimensionless discharge
x	: Runner angular position
γ	: Phase shift throttling pressure
δ	: Phase shift total pressure
θ	: Sensor angular location
φ	: Phase shift runner pressure.

Subscripts

b	: Throttling (pressure)
i	: Harmonic number
k	: Sensor number

r : Rotating (pressure)
 t : Total (pressure).

Data Availability

The data used to support the findings of this study are available from the corresponding author upon request.

Conflicts of Interest

The authors declare no conflicts of interest.

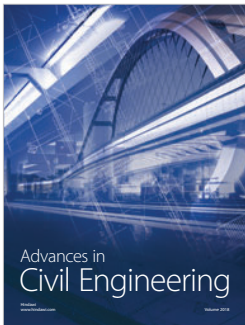
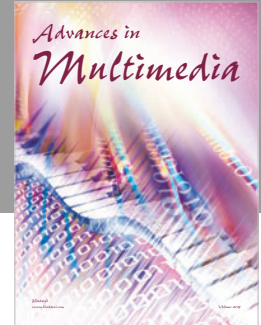
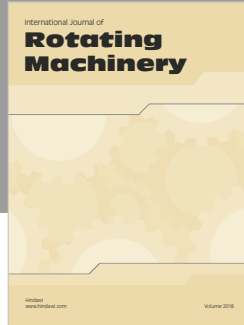
Acknowledgments

This work was funded by Energy Norway, Norwegian Research Council, and the Norwegian Hydropower Center. The authors are grateful for all the support from the technical staff at the Waterpower Laboratory, which was invaluable to make the measurements possible.

References

- [1] S. Lais, Q. Liang, U. Henggeler, T. Weiss, X. Escaler, and E. Egusquiza, "Dynamic analysis of Francis runners-experiment and numerical simulation," *The International Journal of Fluid Machinery and Systems*, vol. 2, no. 4, pp. 303–314, 2009.
- [2] J. Yan, J. Koutnik, U. Seidel, and B. Hubner, "Compressible simulation of rotor-stator interaction in pump-turbines," *The International Journal of Fluid Machinery and Systems*, vol. 3, no. 4, pp. 315–323, 2010.
- [3] L. Xia, Y. Cheng, and F. Cai, "Pressure pulsation characteristics of a model pump-turbine operating in the S-shaped region: CFD simulations," *The International Journal of Fluid Machinery and Systems*, vol. 10, no. 3, pp. 287–295, 2017.

- [4] A. Zobeiri, J.-L. Kueny, M. Farhat, and F. Avellan, "Pump-turbine rotor-stator interactions in generating mode: pressure fluctuation in distributor channel," in *Proceedings of the 23rd IAHR Symposium on Hydraulic Machinery and Systems*, 2006.
- [5] K. Yonezawa, S. Toyahara, S. Motoki, H. Tanaka, P. Doerfler, and Y. Tsujimoto, "Phase resonance in centrifugal fluid machinery," *IJFMS*, vol. 7, no. 2, pp. 42–53, 2014.
- [6] R. Qian, *Flow field measurements in a stator of a hydraulic turbine [Ph.D. thesis]*, Laval University, Laval, Canada, 2008.
- [7] G. D. Ciocan and J. L. Kueny, "Experimental analysis of rotor stator interaction in a pump-turbine," in *Proceedings of the 23rd IAHR Symposium on Hydraulic Machinery and Systems*, Yokohama, Japan, 2006.
- [8] V. Hasmatuchi, *Hydrodynamics of a pump-turbine operating at off-design conditions in generating mode [Doctoral Thesis]*, Ecote Polytechnique Federale de Lausanne, Lausanne, Ecote Polytechnique Federale de Lausanne, Lausanne, Switzerland, 2012.
- [9] P. Dörfler, M. Sick, and A. Coutu, *Flow-Induced Pulsation and Vibration in Hydroelectric Machinery*, Springer, London, UK, 2013.
- [10] Francis-99 NTNU, <https://www.ntnu.edu/nvks/francis-99>.
- [11] IEC, "NEK IEC 60193 Hydraulic turbines, storage pumps and pump-turbines Model acceptance tests," 1999.
- [12] E. Agnalt, P. Østby, B. W. Solemslie, and O. G. Dahlhaug, "Experimental study of a low-specific speed francis model runner during resonance," *Shock and Vibration*, vol. 2018, Article ID 5796875, 12 pages, 2018.
- [13] G. Olimstad, *Characteristics of Reversible Pump-Turbines*, Norwegian University of Science and Technology, NTNU, Trondheim, Norway, 2012.
- [14] R. E. Franklin and J. M. Wallace, "Absolute measurements of static-hole error using flush transducers," *Journal of Fluid Mechanics*, vol. 42, no. 1, pp. 33–48, 1970.
- [15] E. Agnalt, B. W. Solemslie, and O. G. Dahlhaug, "Onboard measurements of pressure pulsations in a low specific speed Francis model runner," in *Proceedings of the 29th IAHR Symposium on Hydraulic Machinery and Systems*, Kyoto, Japan, 2018.
- [16] H. Schlichting and K. Gersten, *Boundary-Layer Theory*, Springer, New York, NY, USA, 9th edition, 2016.



Hindawi

Submit your manuscripts at
www.hindawi.com

